ACES Asian Chemical Editorial Society

DOI: 10.1002/cnma.201700005

CHEMNANOMAT
Communication

Metal Oxide Nanostructures

Synthesis of Cuboctahedral CeO_2 Nanoclusters and Their Assembly into Cuboid Nanoparticles by Oriented Attachment

Santiago Maya-Johnson,[b] Lourdes Gracia,[d] Elson Longo,[a] Juan Andres,[c] and Edson R. Leite*[a]

Abstract: Here, we describe a simple approach to control the oriented attachment process through selective ligand scavenging from the {100} facets of CeO_2 nanoclusters. Aggregates of these nanoclusters smaller than 10 nm with controlled shapes and exposed facets were obtained. For the synthesis of the cuboctahedral CeO_2 nanoclusters, we developed a solvent-controlled synthesis approach based on a non-hydrolytic sol–gel process and used an ester aminolysis reaction to control ligand scavenging from the {100} facets. First-principle calculations allowed us to understand and interpret, at the atomic level, the effects of shape control on the synthesis. Fine-tuning of the desired morphologies can be achieved by controlling the values of the surface energies, which leads to the formation of morphologies that the classic growth process does not allow.

In the last decade, significant progress has been made in the synthesis and assembly of nanocrystals, and has allowed the control of their compositions, sizes, shapes, and functionalities.[1–4] More recently, efforts have focused on the use of non-classical nucleation and growth approaches, which allow the development of nanocrystals and nanoparticles with high complexity in terms of shape, composition, and enhanced functionality.[5–7] An important mechanism related to the non-classical approach is the aggregation of nanoclusters and nanoparticles. Aggregation-based growth (AG) occurs via aggregation and coalescence of nanoclusters or nanocrystals rather than monomer-to-monomer deposition (classical process). Subsequent to aggregation, interface elimination and recrystallization take place.[8] In particular, the AG of stable nanoclusters and nanocrystals with coherent crystallographic orientations, a process known as oriented attachment (OA), is a well-established kinetic process that allows the synthesis of nanoparticles with anisotropic and complex shapes.[9–21]

Since the OA process occurs via collisions between nanocrystals or nanoclusters,[10,22] it can be inhibited by a capping ligand, which protects the nanoparticle surface, through a mechanism similar to steric hindrance. The use of the limited ligand protection method[23] is an elegant way to promote the aggregation of very complex 3D structures. However, this method is not effective for synthesizing nanoparticles with high symmetry and controlled exposed facets. Furthermore, changing the relative concentration of the ligand during the synthesis leads to the variation of the primary nanoparticle size and shape but not their aggregation state.[24–27] Following this line of reasoning, using the OA process to control the nanoscale morphology via the selective removal of the ligand ("ligand scavenger") would be not only be very effective but also be one of the simplest strategies to manipulate the exposed crystallographic facets.

Here, we report a simple and elegant approach to control the OA process using a selective ligand scavenger, which produces nanocluster aggregates smaller than 10 nm with controlled shapes and exposed facets. Cerium oxide (CeO_2) was used as the model system for the development of this growth strategy because it has a cubic symmetry and it is possible to synthesize CeO_2 nanoclusters with well-defined exposed facets, such as cuboctahedral nanoclusters.[24,25] It is interesting to note that a cuboctahedron has the same group symmetry (O_h) as that of a cube. This similarity facilitates the sharing of facets with identical crystallographic orientations during the aggregation process, leading to the formation of aggregates with controlled shapes and exposed facets. The strategy reported here is based on the synthesis of cuboctahedral CeO_2 nanoclusters (see Scheme 1 a) and selective ligand scavenging from their {100} facets (see Scheme 1 b), thereby allowing OA on these surfaces, generating cuboid aggregates. For the synthesis of the cuboctahedral CeO_2 nanoclusters, we developed a solvent-controlled synthesis approach based on a non-hydrolytic sol-

[a] Prof. E. Longo, Prof. E. R. Leite
Department of Chemistry
Federal University of Sao Carlos
13565-905, Sao Carlos, SP (Brazil)
E-mail: edson.leite@pq.cnpq.br

[b] S. Maya-Johnson
Department of Materials Engineering
Federal University of Sao Carlos
13565-905, Sao Carlos, SP (Brazil)

[c] Prof. J. Andres
Department de Química Fisica I Analitica
Universitat Jaume I
12071 Castellon de la Plana (Spain)

[d] Dr. L. Gracia
Department de Química Fisica
Universitat de València
46100 Burjassot (Spain)

Supporting information and the ORCID identification number(s) for the author(s) of this article can be found under http://dx.doi.org/10.1002/cnma.201700005.

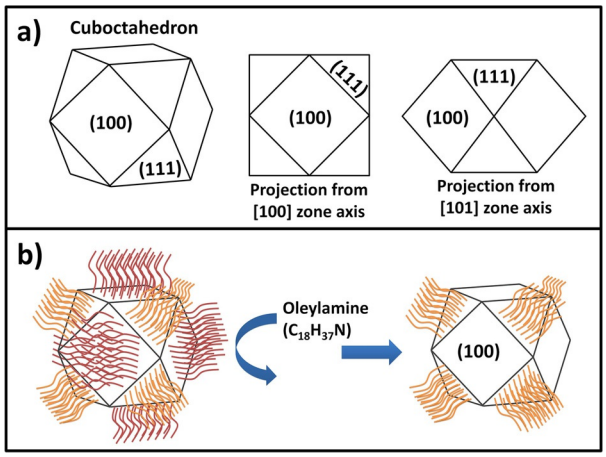

Scheme 1. a) Cuboctahedron with its projections in different zone axis orientations; b) selective ligand scavenger from {100} facets developed in this study.

gel process[25,28] using cerium(III) acetylacetonate hydrate ($Ce(C_5H_7O_2)_3{\cdot}xH_2O$) as the cerium source and oleyl alcohol (OLA) as the solvent and a reactant. For the controlled ligand scavenging from the {100} facets, we used a well-known ester aminolysis reaction.[29]

The detailed experimental procedure used in this work is described in the Supporting Information. We conducted a series of experiments with and without the addition of oleylamine (OAm) (0, 1, 3, or 5 mmol) in order to understand the effect of this primary amine in the selective ligand scavenging.[30] For the synthesis without the addition of OAm, low-magnification high-resolution transmission electron microscopy (HRTEM) images (see Figure S1a in the Supporting Information) revealed the formation of well-dispersed nanoclusters with a mean size of 2.7 nm, and X-ray diffraction (XRD) analysis revealed the crystallization of CeO_2 nanoclusters with a fluorite cubic structure (see Figure S2 in the Supporting Information). HRTEM and XRD analysis showed that the reaction between cerium(III) acetylacetonate and OLA led to the formation of single-crystalline CeO_2 nanoclusters with a well-defined shape and size in the 2–4 nm range.

In order to shed light on the reaction between OLA and the metal precursor, we performed Fourier transform infrared (FTIR) spectroscopy analysis on the CeO_2 nanoclusters (see Figure S3 in the Supporting Information) and identified bands in the 2800–2960 cm^{-1} region attributed to the C–H stretching mode of methyl and methylene groups, a band centered at 3470 cm^{-1} associated with the OH group, and bands at 1544 and 1445 cm^{-1} associated with the stretching of carboxyl groups chemically bonded (as a bidentate complex) to the CeO_2 nanocluster surface.[31] These results show that OLA is oxidized to the carboxylic acid during the synthesis procedure, which acts as a reactant to promote the inorganic phase formation and as a surfactant. At this point, we have to underline that it is quite difficult to clearly determine the reaction mechanism; however, it is clear that a cerium carboxylate complex forms at the nanocluster surface and this carboxylate will act as a surfactant. It is important to note that the CeO_2 nanocluster synthesized without OAm shows very high colloidal stability in organic non-polar solvents, such as hexane and toluene (see Figure S4 in the Supporting Information), supporting the hypothesis that the carboxylate complex acts as a surfactant. Since the CeO_2 nanocluster was synthesized using a high surfactant/cerium precursor ratio, the organic ligand blocked most growth on both the {100} and {111} facets, resulting in the formation of small and truncated octahedral clusters.[24]

Figure 1 shows the nanocluster size distribution of the material synthesized without the addition of OAm, as well as

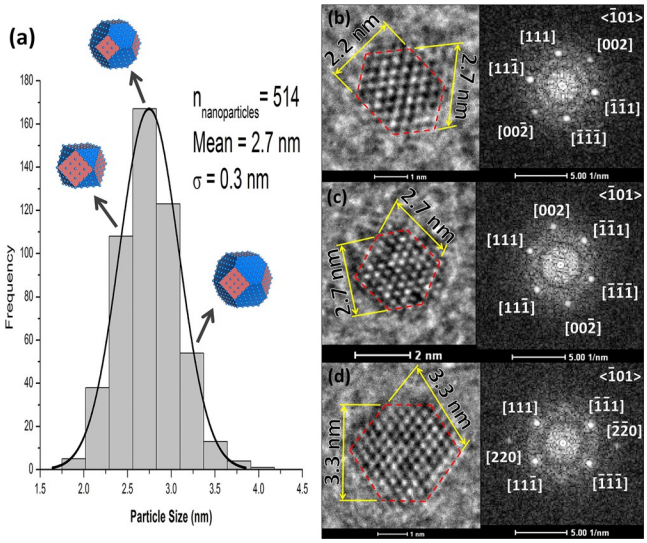

Figure 1. a) Nanocluster size distribution obtained through TEM analysis of the CeO_2 nanoclusters synthesized without (0 mmol) OAm. The arrows indicate that the nanoclusters with different sizes shows different ratio of [100] and [111] facets. Insets (b), (c), and (d) show high-magnification HRTEM images of the similar-sized nanoclusters. FFT analysis showed that the nanoclusters are single-crystal and oriented along the $<\bar{1}01>$ zone axis. Image simulation showed that the CeO_2 nanoclusters have a cuboctahedron shape with {111} and {100} facets.

a series of high-magnification HRTEM images of the well-faceted CeO_2 nanocluster oriented along the $<\bar{1}01>$ zone axis (see the fast Fourier transform (FFT) patterns in the insets). Detailed HRTEM analysis revealed that the nanoclusters show a cuboctahedron shape with {111} and {100} facets. Image simulation of the HRTEM images (see insets in Figure 1a) confirmed the fluorite cubic structure of CeO_2 and showed that the nanoclusters with a mean size of 2.5 nm (Figure 1b) are dominated by {100} facets, with preferential growth in the [111] direction. It is interesting to note that the growth process of the nanoclusters is cyclical, with growth along the [100] direction for nanoclusters with a typical size of 2.7 nm (Figure 1c) and growth along the [111] direction for nanoclusters with a typical size of 3.3 nm (Figure 1d). For more detail, see the video in the Supporting Information. This indicates that the growth of the nanoclusters occurs via classical deposition of monomers with no preferred growth direction, keeping the cuboctahedron shape.

The effect of the addition of OAm on the morphology and aggregation state of the CeO_2 nanoclusters is illustrated in Fig-

ure S1 (Supporting Information). The addition of a small amount of OAm (1 mmol) did not promote any change in the size or aggregation state of the CeO_2 nanoclusters, which kept their cuboctahedron shape (see Figure S1b and particle size distribution in the inset). However, upon increasing the amount of OAm (3 mmol) added to the reaction, we observed a remarkable change in the aggregation state. We noticed the formation of well-defined aggregates of cuboid CeO_2 nanoclusters. Upon increasing the OAm concentration further (5 mmol), we observed the formation of aggregates without defined shapes, indicating the formation of CeO_2 nanocluster agglomerates with random orientation.

In order to obtain a detailed description of the CeO_2 nanocluster aggregates whose formation was promoted by the addition of 3 mmol of OAm, we performed HRTEM characterization with image simulation. Figure 2 shows high-magnification

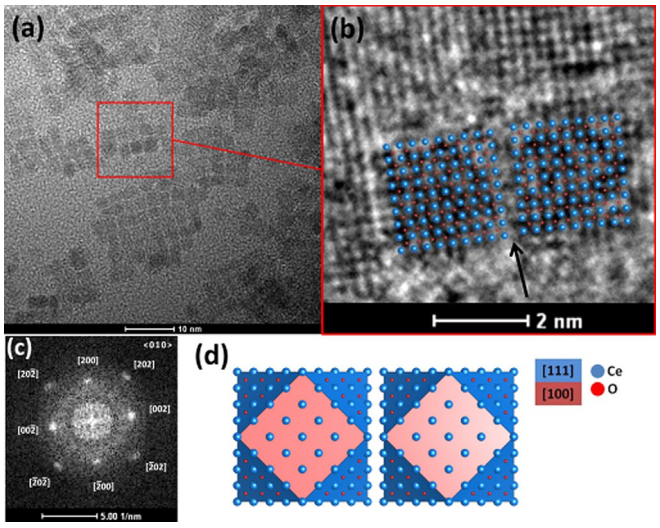

Figure 2. a) High-magnification HRTEM image of the CeO_2 nanocluster aggregates whose formation was promoted by the addition of 3 mmol of OAm; b) detailed view of an ordered aggregate (mesocrystal), where it is possible to observe defects (indicated by arrows) typical of an aggregation promoted by OA; c) FFT of image b; d) image simulation of the CeO_2 nanoclusters showing that aggregates share the {100} facets.

HRTEM images of the cuboid aggregates. Better analysis of this image (Figure 2b and FFT in Figure 2c) revealed that the cuboctahedral CeO_2 nanoclusters share the {100} facets, resulting in a cubic-like structure, oriented along the [001] zone axis, as illustrated in Figure 2d. Furthermore, Figure 2a and Figure 2b strongly suggest that the OA mechanism dominates the AG during the synthesis.[9–22] We can see characteristic defects from the OA aggregation process, such as defects caused by imperfect aggregation between the {100} facets, indicated by the black arrow in Figure 2b, as well as a grain boundary, indicating that the aggregates are in a state of transition from primary nanoclusters to single crystal domain via assembly and recrystallization (we have a mesocrystal).[9,11,15]

The previous HRTEM analysis clearly showed that the OAm modified the aggregation state. With a controlled amount, the addition of OAm resulted in the CeO_2 nanoclusters sharing the {100} facets. This result suggests that the OAm scavenges the carboxylate complex bonded to the {100} surface, allowing the OA process to occur in these facets. A plausible explanation for the role of OAm during the synthesis process is an ester aminolysis reaction that involves the nucleophilic attack of OAm on the carbonyl carbon atom of the cerium carboxylate, as illustrated in Scheme 2. This mechanism is similar to that re-

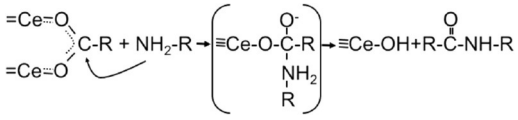

Scheme 2. Aminolysis reaction between a carboxylate complex bonded to the CeO_2 surface and OAm.

ported by Han for the synthesis of titania nanorods with tunable aspect ratios.[29] The removal of the carboxylate complex from the nanocluster surface was confirmed by thermogravimetric analysis (TGA) of the CeO_2 nanoclusters synthesized with and without OAm. As we can see in the TGA results shown in Figure S5 (see Supporting Information), the nanocluster synthesized in the presence of OAm showed less weight loss, confirming the partial removal of the carboxylate complex from the CeO_2 nanoclusters. FTIR analysis (see Figure S3 in the Supporting Information) did not produce any signs of amine groups in the nanocluster synthesized with OAm, indicating that this compound promotes only the removal of the ligand. In the present study, the selective removal of the carboxylate complex from the {100} facets and the formation of hydroxylated cerium on the surface allowed the subsequent nanocluster aggregation to occur via OA in a controlled manner. The selective removal of the ligand will eliminate the steric hindrance in the [100] direction.

The results reported thus far clearly show that the surface energies of the different CeO_2 facets play a crucial role in both classical and non-classical growth processes. To obtain an understanding from an energetic point of view, we performed first-principle calculations for the different CeO_2 surfaces (for details about the theoretical methodology used, see the theoretical calculation procedure in the Supporting Information). The {100}, {110}, and {111} facets of CeO_2 were modeled by an unreconstructed slab model using an optimized equilibrium geometry. Slab models (see Figure S6 in the Supporting Information) containing 8, 7, and 7 molecular units were considered for the {100}, {110}, and {111} facets, respectively, after some convergence tests were performed on the system. Their respective areas were 14.4, 20.7, and 12.6 $Å^2$. According to the theoretical calculations, the {111} facet was the most stable, followed by the {110} and then the {100} facets. In principle, a stable crystal system tends to expose the facets with the lowest surface energy. The ideal morphology of CeO_2, derived from the Wulff construction, exhibits a typically octahedral shape exposing the {111} facets. The calculated surface energies are shown in the inset of Figure 3a.

Our theoretical calculation approach, based on the Wulff construction, allows the modification of the morphology by

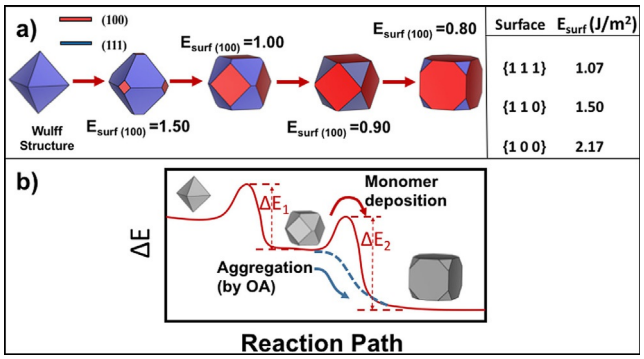

Figure 3. a) Morphology simulation for the theoretically calculated {100} and {111} surface energies of CeO_2. The inset shows the surface energy obtained through the first-principle calculations; b) description of the reaction pathway for the classical and non-classical growth processes.

tuning the surface energies of the different facets (see Figure S7 in the Supporting Information). Analysis of the theoretical results revealed that when the relative stability of the facets changes (increases or decreases), more than one type of facet will appear in the resulting morphology. The available morphologies shown in Figure 3a reflect a change in the {100} surface energy. To generate a cuboctahedron with exposed {100} and {111} surfaces, it is necessary to decrease the surface energy of the {100} facets. It is also clear from our simulation study that to obtain a cuboid shape, it is necessary to decrease the surface energy of the {100} surfaces further. Therefore, to obtain a cube-like nanocrystal or nanocluster, it is necessary to change the surface energy of the {100} facets, which will result in preferential growth in the [111] direction. Thus, the reduction of the surface energy serves as a driving force for the OA growth process.[32]

The ratio between the surface energies of the (111) and (100) facets (see Figure S8 in the Supporting Information) is a useful parameter for understanding the growth process. This ratio for the Wulff structure is 0.49 and the ratio for a cubic morphology is 1.73. From this theoretical analysis, it is clear that to obtain morphologies with {001} facets, it is necessary to alter the surface energy of these facets. Therefore, the change in the morphology of the CeO_2 nanocrystals from truncated octahedral to cubic was mostly caused by the suppression of crystal growth on the {100} surface.[20] As the CeO_2 {100} surfaces are less stable than the {111} surfaces, the carboxylate ligands interact preferentially with the {100} surfaces. This reduced the growth rate of the crystals in the {100} direction significantly, and the crystal growth in the {111} direction became dominant. The change in growth direction led to the formation of nanocubes with exposed {100} surfaces.

The morphology change can be attributed to the fluctuation of the energy barriers for the formation of different crystal facets during nanocrystal growth. In our case, if the difference between the surface energies for the {100} facets in the initial and final morphologies are considered as kinetic energy barriers (ΔE_1 and ΔE_2 in Figure 3b), then we can conclude that the carboxylate complex bonded to the nanocluster surface decreased the surface energy of the {100} facets sufficiently to allow the kinetic barrier, ΔE_1, to be overcome, and a cuboctahedron with {111} and {100} facets was formed. However, we did not observe (under the experimental conditions used) the formation of cubic nanoclusters experimentally, suggesting that the stabilization of the surface by the complex did not promote a sufficient reduction of the surface energy of the {100} facets to cause the formation of a cubic morphology, i.e., to overcome the ΔE_2 barrier. However, the addition of OAm led to selective scavenging of the ligand from the {100} surfaces, allowing the OA process to occur on these surfaces. This event allowed the formation of cubic nanoparticles, following an OA non-classical growth process. The attachment between nanoclusters, via OA, should result in a significant reduction in the surface energies of the connected facets, thus allowing the formation of morphologies that the classic growth process (monomer deposition) does not allow. This is equivalent to finding a reaction path that can overcome the kinetic energy barrier (ΔE_2), as illustrated in Figure 3b.

In summary, based on both experimental and theoretical results, we have reported here a reaction pathway that allowed the use of the OA process in a controlled fashion for the synthesis of CeO_2 nanoparticles with controlled sizes and shapes via a control ligand scavenging process involving the {100} facets selectively. First-principle calculations were carried out to understand and interpret, at the atomic level, the structure, surface stability, and morphological transformations; the surface energies of the connected facets were reduced significantly, enabling the formation of morphologies that the classic growth process does not allow. The methodology reported here for the synthesis of CeO_2 may be relevant for the investigation of self-assembly processes of other metal oxides as well as for other types of inorganic nanoparticles in future work, which means that it brings new insight for nanostructure design and controlled synthesis.

Acknowledgements

This research was conducted with the financial support of FAPESP (CEPID project 2013/07296-2), FINEP, CNPq, and CAPES (all Brazilian agencies); Generalitat Valenciana for PrometeoII/2014/022; ACOMP/2014/270; ACOMP/2015/1202; Ministerio de Economia *y* Competitividad, project CTQ2015-65207-P (all Spanish agencies); and Programa de Cooperación Científica con Iberoamerica (Brasil) of the Ministerio de Educación (PHBP14-00020). J. A. acknowledges the Ministerio de Economia *y* Competitividad, "Salvador Madariaga" program, PRX15/00261. Santiago Maya acknowledges Bruno H. R. Lima and Ricardo H. Gonçalves for the stimulating discussions.

Keywords: ceria · nanoclusters · non-classic growth · non-hydrolytic synthesis · oriented attachment

[1] Y. Yin, A. P. Alivisatos, *Nature* **2005**, *437*, 664 – 670.
[2] M. V. Kovalenko, L. Manna, A. Cabot, Z. Hens, D. V. Talapin, C. R. Kagan, V. I. Klimov, A. L. Rogach, P. Reiss, D. J. Milliron, P. Guyot-Sionnnest, G. Konstantatos, W. J. Parak, T. Hyeon, B. A. Korgel, C. B. Murray, W. Heiss, *ACS Nano* **2015**, *9*, 1012 – 1057.

[3] C. K. Kim, T. Kim, I.-Y. Choi, M. Soh, D. Kim, Y.-J. Kim, H. Jang, H.-S. Yang, J. Y. Kim, H.-K. Park, S. P. Park, T. Yu, B. W. Yoon, S. H. Lee, T. Hyeon, *Angew. Chem. Int. Ed.* **2012**, *51*, 11039 – 11043; *Angew. Chem.* **2012**, *124*, 11201 – 11205.
[4] K. Bhargava, A. Arya, A. Gangwar, S. Singh, M. Roy, M. Das, N. Sethy, *Int. J. Nanomed.* **2016**, 1159.
[5] J. Lee, J. Yang, S. G. Kwon, T. Hyeon, *Nat. Rev. Mater.* **2016**, *1*, 16034.
[6] S. A. Hassan, *J. Chem. Phys.* **2011**, *134*, 114508.
[7] H. Zhang, J. F. Banfield, *J. Phys. Chem. Lett.* **2012**, *3*, 2882 – 2886.
[8] H. Zhang, J. J. De Yoreo, J. F. Banfield, *ACS Nano* **2014**, *8*, 6526 – 6530.
[9] V. M. Yuwono, N. D. Burrows, J. A. Soltis, R. L. Penn, *J. Am. Chem. Soc.* **2010**, *132*, 2163 – 2165.
[10] D. Li, M. H. Nielsen, J. R. I. Lee, C. Frandsen, J. F. Banfield, J. J. D. Yoreo, *Science* **2012**, *336*, 1014 – 1018.
[11] R. L. Penn, J. F. Banfield, *Science* **1998**, *281*, 969 – 971.
[12] H. Cölfen, M. Antonietti, *Angew. Chem. Int. Ed.* **2005**, *44*, 5576 – 5591; *Angew. Chem.* **2005**, *117*, 5714 – 5730.
[13] H. Cölfen, M. Antonietti, *Mesocrystals and Nonclassical Crystallization*, Wiley, Chichester, West Sussex, England, **2008**.
[14] R. L. Penn, J. F. Banfield, *Am. Mineral.* **1998**, *83*, 1077 – 1082.
[15] R. O. Da Silva, R. H. Gonçalves, D. G. Stroppa, A. J. Ramirez, E. R. Leite, *Nanoscale* **2011**, *3*, 1910.
[16] X. Xue, R. L. Penn, E. R. Leite, F. Huang, Z. Lin, *CrystEngComm* **2014**, *16*, 1419.
[17] E. J. H. Lee, C. Ribeiro, E. Longo, E. R. Leite, *J. Phys. Chem. B* **2005**, *109*, 20842 – 20846.
[18] J. J. De Yoreo, P. U. P. A. Gilbert, N. A. J. M. Sommerdijk, R. L. Penn, S. Whitelam, D. Joester, H. Zhang, J. D. Rimer, A. Navrotsky, J. F. Banfield, et al., *Science* **2015**, *349*, aaa6760.
[19] W. Lv, W. He, X. Wang, Y. Niu, H. Cao, J. H. Dickerson, Z. Wang, *Nanoscale* **2014**, *6*, 2531.
[20] H. Zhang, J. F. Banfield, *CrystEngComm* **2014**, *16*, 1568 – 1578.
[21] J. Zhang, F. Huang, Z. Lin, *Nanoscale* **2010**, *2*, 18 – 34.
[22] C. J. Dalmaschio, C. Ribeiro, E. R. Leite, *Nanoscale* **2010**, *2*, 2336.
[23] A. Narayanaswamy, H. Xu, N. Pradhan, X. Peng, *Angew. Chem. Int. Ed.* **2006**, *45*, 5361 – 5364; *Angew. Chem.* **2006**, *118*, 5487 – 5490.
[24] J. Zhang, S. Ohara, M. Umetsu, T. Naka, Y. Hatakeyama, T. Adschiri, *Adv. Mater.* **2007**, *19*, 203 – 206.
[25] S. S. Lee, H. Zhu, E. Q. Contreras, A. Prakash, H. L. Puppala, V. L. Colvin, *Chem. Mater.* **2012**, *24*, 424 – 432.
[26] T. Yu, J. Joo, Y. I. Park, T. Hyeon, *Angew. Chem. Int. Ed.* **2005**, *44*, 7411 – 7414; *Angew. Chem.* **2005**, *117*, 7577 – 7580.
[27] M. A. L. Cordeiro, W. Wenig, D. Stroppa, C. J. Kiely, E. R. Leite, *Chem. Mater.* **2013**, *25*, 2028 – 2034.
[28] M. Niederberger, N. Pinna, *Metal Oxide Nanoparticles in Organic Solvents*, Springer, London, **2009**.
[29] Z. Zhang, X. Zhong, S. Liu, D. Li, M. Han, *Angew. Chem. Int. Ed.* **2005**, *44*, 3466 – 3470; *Angew. Chem.* **2005**, *117*, 3532 – 3536.
[30] S. Mourdikoudis, L. M. Liz-Marzán, *Chem. Mater.* **2013**, *25*, 1465 – 1476.
[31] C. Slostowski, S. Marre, O. Babot, T. Toupance, C. Aymonier, *Langmuir* **2012**, *28*, 16656 – 16663.
[32] R. L. Penn, *J. Phys. Chem. B* **2004**, *108*, 12707 – 12712.

Manuscript received: January 10, 2017
Accepted Article published: February 6, 2017
Final Article published: February 23, 2017